NASA TN D-907

TECHNICAL NOTE

D-907

LOCAL AERODYNAMIC HEAT TRANSFER AND BOUNDARY-LAYER TRANSITION ON ROUGHENED SPHERE-ELLIPSOID BODIES AT MACH NUMBER 3.0

By William D. Deveikis and Robert W. Walker

Langley Research Center
Langley Field, Va.

NATIONAL AERONAUTICS AND SPACE ADMINISTRATION
WASHINGTON

August 1961

NATIONAL AERONAUTICS AND SPACE ADMINISTRATION

TECHNICAL NOTE D-907

LOCAL AERODYNAMIC HEAT TRANSFER AND BOUNDARY-LAYER TRANSITION ON ROUGHENED SPHERE-ELLIPSOID BODIES AT MACH NUMBER 3.0

By William D. Deveikis and Robert W. Walker

SUMMARY

A wind-tunnel investigation was made to determine heat-transfer distributions on three steel sphere-ellipsoid bodies with surface roughnesses of 5, 100, and 200 microinches. Tests were conducted in the Langley 9- by 6-foot thermal structures tunnel at a Mach number of 3.0, free-stream Reynolds numbers (based on model spherical diameter) of 4.25×10^6 and 2.76×10^6, and at a stagnation temperature of 650° F. Pressure distributions were obtained also on a fourth model. The results indicated that the combination of surface roughness and boundary-layer cooling tended to promote early transition and nullify the advantages attributable to the blunt shape of the model for reducing local temperatures. Good correlation between experimental heating rates and those calculated from laminar theory was achieved up to the start of boundary-layer transition. The correlation also was good with the values predicted by turbulent theory for surface stations downstream from the 45° station.

INTRODUCTION

The present investigation was conducted to determine the effects of surface roughness on the heat-transfer distribution over the plastic sphere-ellipsoid models of reference 1. In that investigation, wind-tunnel airstream contamination roughened the model surfaces to a degree which was believed to have affected the location of boundary-layer transition and, hence, the region of maximum aerodynamic heating input. Inasmuch as instrumentation limitations imposed on the plastic models by structural considerations precluded direct measurement of the heat-transfer distributions, steel models having different surface roughnesses were constructed and tested.

Four models were tested simultaneously in the Langley 9- by 6-foot thermal structures tunnel at a Mach number of 3.0, at free-stream Reynolds numbers (based on model spherical diameter) of 4.25×10^6 and 2.76×10^6, and at a stagnation temperature of 650° F. Three of the models were instrumented with thermocouples in order to obtain heat-transfer data, and the fourth model was used to obtain pressure distributions. The pressure-distribution model and one heat-transfer model had a surface finish of 5 microinches. The other heat-transfer models were finished to average surface roughness values of 100 and 200 microinches, respectively, in order to cover the range of surface roughness conditions estimated for the plastic models of reference 1. A discussion and analysis of the results are presented herein.

SYMBOLS

C_p pressure coefficient

c_m specific heat of model wall material

c_p specific heat of air at constant pressure

D model spherical diameter

h local heat-transfer coefficient, $\frac{q_w}{T_r - T_w}$

k thermal conductivity for air

N_{Nu} Nusselt number, $\frac{hD}{k}$

N_{Pr} Prandtl number, $\frac{c_p \mu}{k}$

N_{St} Stanton number, $\frac{h}{\rho v c_p}$

p pressure

q heat flow rate per unit area

R_D Reynolds number whose characteristic length is D, $\frac{\rho v D}{\mu}$

R_s local Reynolds number, $\frac{\rho v s}{\mu}$

r	local radius perpendicular to model longitudinal axis
s	surface distance from stagnation point
T	temperature
t	time
v	velocity
w	specific weight of model wall material
x	axial distance from stagnation point
β	velocity gradient along the surface, $\frac{\partial v}{\partial s}$
θ	angular distance around models measured from the stagnation point in spherical polar coordinate system
μ	absolute viscosity of air
ρ	mass density of air
τ	model wall thickness

Subscripts:

D	parameter based on model spherical diameter as characteristic length
l	local free-stream conditions evaluated at outer edge of boundary layer
o	initial conditions
r	recovery, surface conditions
s	parameter based on surface distance as characteristic length
t	stagnation conditions
w	outside wall of model
σ	free-stream conditions evaluated immediately behind bow shock wave
∞	free-stream conditions ahead of shock wave

SPECIMENS, APPARATUS, AND TESTS

Models

Principal model dimensions are shown in figure 1. The models were machined to the same size and profile as the plastic sphere-ellipsoid models of reference 1. Integral with the models was a conical skirt with a flare angle of approximately 5° which extended to a base diameter of 5.75 inches. Model wall thickness was 0.030 inch for the heat-transfer models and approximately 0.12 inch for the pressure model. Heat-transfer model wall-thickness variations were held within ±0.001 inch. The outer surfaces of two of the heat-transfer models were sandblasted to average roughnesses of approximately 100 and 200 microinches, respectively. The outer surfaces of the third heat-transfer model and the pressure model were polished to a finish of approximately 5 microinches. Average roughness heights of the model surfaces were measured with a Physicists Research Company Profilometer. In order to prevent large changes in model surface roughness during the tests, the models were machined from a hard material (SAE 1020 carbon steel). Precautions were also taken to minimize the amount of foreign particles in the airstream by the installation of a fine mesh screen at the upstream end of the tunnel nozzle entrance cone. The nozzle and test-section areas were also vacuum cleaned prior to each test to remove dust and sand that might have been sucked into the tunnel during the shutdown period of the previous test.

L 1 3 9 3

Instrumentation for the heat-transfer models consisted of 14 No. 30 gage iron constantan thermocouples spot-welded to the inner surface of each model. The thermocouples were staggered along two meridians 180° apart emanating from the stagnation point. Thermocouple surface station locations are tabulated in figure 1. The pressure-distribution model contained 18 pressure orifices 0.070 inch in diameter. Eight orifices were arranged in a spiral of one revolution around the model and were located at the surface stations tabulated in figure 1. At stations 1.00 and 2.27 and on the conical skirt, there were four orifices equally spaced around the circumference. Model pressures and temperatures were recorded by means of a high-speed digital magnetic tape recording system.

Test Facility

The tests were conducted in the Langley 9- by 6-foot thermal structures tunnel, an intermittent supersonic blowdown facility exhausting to the atmosphere. Air for the facility is dried to a dewpoint of -40° F and stored in a large tank field at a pressure of 450 pounds per square inch absolute. Four quick-acting rotary valves automatically control the air from the storage field to provide preset stagnation pressures from a

minimum starting pressure of 120 pounds per square inch absolute to a maximum of 200 pounds per square inch absolute. Stagnation temperatures up to approximately 660° F are obtained by passing the air through a stainless-steel heat exchanger which is preheated by an oil-fired indirect air heater. The air then passes through a two-dimensional supersonic nozzle designed for a test section Mach number of 3.0.

The test section is 6 feet high, 8 feet 9 inches wide, and 10 feet long. Calibration tests have shown that the maximum deviation in test section Mach number is less than 1.0 percent. Flow conditions and running times available in the test section are given in the following table:

Mach number	3.0			
Reynolds number per foot	6.6×10^6 to 19×10^6			
Dynamic pressure, lb/sq ft	3,000 to 5,000			
Stagnation temperature, °F	300 to 660		300 to 660	
Maximum running times for constant T_t, sec	23	28	15	18
Maximum running times for constant p_t, sec	40	48	18	22

The lower stagnation temperature limit of 300° F is imposed to avoid the possibility of condensation in the test section. The running times listed are the maximum times for which either the stagnation pressure or stagnation temperature can be held constant. Running times for which stagnation temperature is held constant are based on a temperature drop of not more than 10° F. All times shown in the table are exclusive of the starting and shutdown periods of 2 seconds and 7 seconds, respectively. During these periods, the flow separates from the nozzle walls and subjects the test specimens to unsteady loads considerably in excess of the aerodynamic loads applied under test conditions.

Model Installation

All four models were tested simultaneously. Each model was attached to a cylindrical mounting bucket at the end of a short strut as shown in figure 2. The heat-transfer models were mounted from the upper test-section wall with the thermocouples oriented in a vertical plane. The pressure model was mounted off a side wall. All models were located at the same tunnel longitudinal station at zero angle of attack and yaw with respect to the tunnel longitudinal center line.

Test Conditions

Two tests were performed. Test conditions were selected to cover the limits of the range of conditions imposed during the tests of reference 1. Free-stream Reynolds numbers (based on model spherical diameter) were 4.25×10^6 and 2.76×10^6. Tunnel stagnation pressures were 202 and 132 lb/sq in. abs, and the stagnation temperature was 650° F. The duration of test conditions for the high Reynolds number test was 18.5 seconds, whereas the lower Reynolds number permitted extending this period to 26.2 seconds. These values are exclusive of the starting and shutdown periods of 2 seconds and 7 seconds, respectively.

RESULTS AND DISCUSSION

The condition of the model surfaces after the tests showed that the airstream contamination had largely been eliminated. Profilometer readings taken on the heat-transfer and pressure model with an initial surface roughness of 5 microinches showed that the surface finish changed by only 20 microinches.

Model Pressures

Pressures measured along the sphere-ellipsoid surface and conical skirt at the two free-stream Reynolds numbers of this investigation are shown in figure 3 as the ratio of local to stagnation-point pressure. The measured pressures are compared with the pressures calculated from modified Newtonian theory given by the relation

$$C_p = C_{p,\sigma} \cos^2\theta$$

As shown in figure 3, the measured pressures are closely approximated by the theoretical values over most of the surface. Consequently, isentropic flow relations and the modified Newtonian pressure distribution were used in calculating the local flow conditions required in the analysis of the heat-transfer data discussed in the appendix.

Temperature Distributions

Temperature data were obtained from all three heat-transfer models during the high Reynolds number test, but extensive instrumentation system failures occurred in both the smooth model and the model with a surface roughness of 100 microinches during the low Reynolds number

test. Consequently, only the data obtained from the model with a surface roughness of 200 microinches are reported for the low Reynolds number test.

Typical surface-temperature distributions obtained from each model at various times during the high Reynolds number test are shown in figure 4. The sharp rise in temperature noted downstream from the stagnation point in figure 4 is characteristic of boundary-layer transition to turbulent flow. As the test progressed, the peak in the curves gradually diminished to the relatively flat distribution shown for $t = 18$ seconds. In general, equilibrium temperatures were achieved just before the end of test conditions.

The Effect of Surface Roughness on Heat-Transfer Distribution

Experimental heat-transfer results obtained early in the tests from each model are plotted in figure 5 as the distribution along the surface of the laminar heat-transfer parameter, $N_{St,\infty}\sqrt{R_{D,\infty}}$. The airflow properties used were the undisturbed free-stream conditions, and model spherical diameter was taken as the characteristic length. Also shown in figure 5 are theoretical curves for both laminar and turbulent boundary layers. The curves were calculated from the modifications of Sibulkin's and Falkner's theories given in references 2 and 3. The procedures used in determining the experimental heat-transfer coefficients and theoretical values of the parameter are discussed in the appendix. Errors in the experimental heat-transfer coefficients introduced by conduction effects were evaluated at surface stations where these effects were considered to be greatest by using the method given in reference 3. Since the maximum change in heat-transfer coefficient at these stations varied from approximately 6 to 8 percent and the average change at other stations was less than 4 percent, the effects of conduction were neglected. Heat losses due to radiation were also evaluated and considered small enough to neglect.

The experimental heat-transfer distributions shown in figure 5 indicate that all three models experienced transition to turbulent flow as evidenced by the abrupt departure from the trend of the laminar theory curve. The most evident effect of surface roughness is the familiar upstream shift in the location of boundary-layer transition. For these models, the start of transition moved from the vicinity of the sphere-ellipsoid junction (a station 45° from the stagnation point) on the smooth model to a position just downstream from the stagnation point on the roughest model. The indicated shift in the location of the start

of transition between the models with surface roughnesses of 5 and 100 microinches was greater than the shift shown between the models with surface roughnesses of 100 and 200 microinches. Accompanying this upstream shift in the location of transition due to roughness is an increase in peak heating rates. For the model with a surface roughness of 200 microinches, these heating rates attained values approximately twice the stagnation-point value.

The good agreement between the experimental values and the values obtained from laminar theory up to the start of transition, as seen in figure 5, indicates the adequacy of the theory for predicting laminar heat-transfer distributions for the bodies tested in this investigation. Also, the agreement between experimental values and the values given by turbulent theory is good at surface stations downstream from the sphere-ellipsoid junction.

In the present investigation, stagnation-point values of the parameter, $N_{St,\infty}\sqrt{R_{D,\infty}}$, were not obtained for the two roughest models (see fig. 5), and a comparison cannot be made to ascertain differences in stagnation-point heating due to roughness. However, a direct comparison of the values of the heat-transfer parameter on the three models can be made in figure 5(a) at surface station, $\frac{s}{D} = 0.056$, just downstream from the stagnation point. Although the value of the parameter, $N_{St,\infty}\sqrt{R_{D,\infty}}$, is highest for the roughest model, this may indicate only that the flow is not laminar at that station. Reference to figures 5(a) and 5(b) shows an increase in the heat-transfer parameter with increase in free-stream Reynolds number for the roughest model (200 microinches surface roughness) at surface station, $\frac{s}{D} = 0.056$. In reference 4, an increase in the laminar heating rate with increase in free-stream Reynolds number was observed on a roughened hemisphere-cone-cylinder. For the present investigation, however, there is no assurance that an increase in the laminar heating rate is represented for the test made at the higher Reynolds number.

Boundary-Layer Transition Reversal

In determining experimental local heat-transfer coefficients, two values were obtained for each model at surface stations in the vicinity of initial peak heating rates shown in figure 5. For these stations, a decrease in heat-transfer coefficient occurred when the model wall temperature attained a certain value. The wall temperature at which the reduction in heat-transfer coefficient took place increased as the surface distance measured from the stagnation point increased. This effect

is illustrated in figure 6, where the wall-to-free-stream temperature ratio for reduction in heating rate is plotted against free-stream Reynolds number with surface distance, s, as characteristic length. As shown in figure 6, the wall-to-free-stream temperature ratio varied from approximately 2.33 to 2.67, depending on the surface roughness and surface distance. For the model with a surface roughness of 200 microinches, the wall temperature ratio for reduction in heating rate was found independent of the free-stream Reynolds number based on model spherical diameter and also appeared to approach a constant value.

The change in heat-transfer distributions due to the lower heating rates is shown in figure 7, where the values of the parameter, $N_{St,\infty}\sqrt{R_{D,\infty}}$, obtained later in the tests are shown as the closed symbols. For the smooth model (5 microinches surface roughness) at $R_{D,\infty} = 4.25 \times 10^6$ (fig. 7(c)) and the roughest model (200 microinches surface roughness) at $R_{D,\infty} = 2.76 \times 10^6$ (fig. 7(d)), the reduction in heat-transfer coefficient was sufficient to conclude that the flow had changed from turbulent to laminar. Thus, the transition point moved downstream after an increase in model wall temperature. A comparison of the conditions at which the downstream movement of transition first occurred on the smooth model tested at the high Reynolds number (see fig. 7(c), surface station $\frac{s}{D} = 0.333$) with those of the roughest model tested at the lower Reynolds number (see fig. 7(d), surface station $\frac{s}{D} = 0.167$) showed that the local pressures and model wall temperatures at these two surface stations were nearly the same.

A downstream shift in the location of transition on smooth blunt bodies with increase in surface temperature was also observed during tests reported in references 4 to 6. This behavior, known as transition reversal, has been the subject of considerable interest (see, for example, refs. 4 to 9), and its cause is not yet thoroughly understood. The chief point of controversy is centered on whether the apparent boundary-layer destabilizing effect of extreme surface cooling is of a nonroughness origin. (See, for example, ref. 8.) In reference 6, it was concluded, on the basis of calculations of the minimum roughness height required to excite transition, that roughness was not the dominant factor in causing the initially turbulent flow during the hemisphere tests of that investigation. On the other hand, in reference 7 it was shown experimentally that transition can result directly from the effects of roughness in a cooled boundary layer. For the present investigation, it is clear that the combination of surface roughness and boundary-layer cooling tended to promote early transition to turbulent flow and nullify the advantages attributed to the bluntness of the model shape in reducing local temperatures.

CONCLUSIONS

An investigation to determine the heat-transfer distribution on a sphere-ellipsoid body for three surface roughness conditions was conducted in the Langley 9- by 6-foot thermal structures tunnel. Three thermocouple instrumented steel models were constructed with surface finishes of 5, 100, and 200 microinches, respectively. The models were tested simultaneously at Mach number 3.0, free-stream Reynolds numbers (based on model spherical diameter) of 4.25×10^6 and 2.76×10^6, and a stagnation temperature of approximately 650° F. Local pressures were measured on a fourth model. The test results indicated the following:

1. As surface roughness increased, the location of the start of boundary-layer transition shifted from a station 45° from the stagnation point on the smooth model (5 microinches surface roughness) to a position just downstream from the stagnation point on the roughest model (200 microinches surface roughness). A greater difference in the location of transition was observed between the smooth model (5 microinches surface roughness) and the model with a surface roughness of 100 microinches than between the two roughest models (100 and 200 microinches surface roughness). The differences in location of the start of transition due to roughness were accompanied by an increase in peak heating rates which attained values approximately twice the stagnation-point value for the roughest model.

2. As the model surface temperature reached certain values, a decrease in heat-transfer coefficient occurred on all models at surface stations in the vicinity of initial peak heating rates. The wall-to-free-stream temperature ratio at which the reduction in heating rate occurred increased as the surface distance from the stagnation point increased and varied from approximately 2.33 to 2.67. The reduction in heat-transfer coefficient was sufficient to conclude that the location of boundary-layer transition had moved downstream on the smooth model for the high Reynolds number test and on the roughest model for the low Reynolds number test.

3. In general, the measured pressure distributions over the model were in good agreement with those predicted by modified Newtonian theory.

4. Theoretical heat-transfer distributions for laminar flow using modifications of Sibulkin's theory were in good agreement with experimental distributions up to the start of transition. Also, theoretical heat-transfer values for turbulent flow using a modification of Falkner's theory were in good agreement with experimental values at surface stations downstream from the sphere-ellipsoid junction.

Langley Research Center,
National Aeronautics and Space Administration,
Langley Field, Va., April 13, 1961.

APPENDIX

DATA REDUCTION AND THEORIES

Experimental Heat-Transfer Coefficients

Local heat-transfer coefficients were determined from the slope of the straight-line variation of the measured temperature plotted against its time rate of change in the heat-balance equation

$$c_m w\tau \frac{dT_w}{dt} = h(T_r - T_w) \tag{1}$$

where h and T_r are assumed constant for a given set of test conditions. In equation (1) T_r is the intercept on the T_w axis when T_w is plotted against $\frac{dt_w}{dt}$. In order to ensure against using data influenced by irregularities in test conditions, no data were considered in the analysis at times below 2.5 seconds. At some surface stations, two straight-line variations of T_w with $\frac{dT_w}{dt}$ were obtained as shown in figure 8. Using the slopes of each straight line, two values of h were computed. This indicated the existence of the transition reversal phenomenon in these tests as shown in figure 7. The value of h obtained in this manner was checked by computing temperature variations with time at each station from the solution to the differential equation (1) given by the relation

$$\frac{T_w - T_o}{T_r - T_o} = 1 - e^{-\frac{ht}{c_m w\tau}} \tag{2}$$

The difference between computed and measured temperatures was always within 2 percent of $(T_r - T_o)$. Physical constants used in the data reduction were $c_m = 0.129$ Btu/(lb)($^\circ$F) and $w = 490$ lb/cu ft.

Heat-Transfer Parameter

Stagnation point.- The curves labelled "laminar theory" in figures 5 and 7 were computed from modifications of Sibulkin's theory given in

reference 2 for a hemisphere-cylinder. A stagnation-point solution was presented in reference 2 in terms of the Nusselt number and Reynolds number based on spherical diameter and physical properties of the air evaluated immediately behind the normal shock. The theoretical heat-transfer parameter obtained is a function of Prandtl number and velocity gradient along the surface as follows:

$$\frac{N_{Nu,D,\sigma}}{\sqrt{R_{D,\sigma}}} = 0.763\left(N_{Pr,\sigma}\right)^{2/5}\left(\frac{\beta D}{v_\sigma}\right)^{1/2} \tag{3}$$

By expressing this solution as the product of the Stanton number and the square root of the Reynolds number, equation (3) becomes

$$N_{St,\sigma}\sqrt{R_{D,\sigma}} = \frac{N_{Nu,D,\sigma}}{N_{Pr,\sigma}\sqrt{R_{D,\sigma}}} = 0.763\left(N_{Pr,\sigma}\right)^{-3/5}\left(\frac{\beta D}{v_\sigma}\right)^{1/2} \tag{4}$$

Transformation to undisturbed free-stream conditions required multiplying both sides of equation (4) by the product,

$$\left(\frac{c_{p,\sigma}}{c_{p,\infty}}\right)\left(\frac{\rho_\sigma v_\sigma \mu_\sigma}{\rho_\infty v_\infty \mu_\infty}\right)^{1/2}$$

Equation (4) can then be written as

$$N_{St,\infty}\sqrt{R_{D,\infty}} = \frac{h}{\rho_\infty v_\infty c_{p,\infty}}\sqrt{\frac{\rho_\infty v_\infty D}{\mu_\infty}} = 0.763\left(N_{Pr,\sigma}\right)^{-3/5}\left(\frac{\beta D}{v_\sigma}\right)^{1/2}\left(\frac{c_{p,\sigma}}{c_{p,\infty}}\right)\left(\frac{\rho_\sigma v_\sigma \mu_\sigma}{\rho_\infty v_\infty \mu_\infty}\right)^{1/2} \tag{5}$$

Using isentropic-flow relations and a value of $\frac{\beta D}{v_\sigma} = 4.97$ determined from modified Newtonian theory, a stagnation-point value of $N_{St,\infty}\sqrt{R_{D,\infty}} = 3.44$ is obtained. This value is in agreement with that computed at the stagnation point of a hemisphere-cone-cylinder in reference 4.

Laminar flow.- In reference 2, a relation is given for the local Stanton number which should be valid for stations up to 45° from the stagnation point or $\frac{s}{D} = 0.393$. The relation, also based on a modification of Sibulkin's theory, uses physical properties of the air evaluated at the outer edge of the boundary layer and s as characteristic length as follows:

$$N_{St,l}\sqrt{R_s} = 0.763\left(N_{Pr,l}\right)^{-3/5} \tag{6}$$

Transformation to undisturbed free-stream conditions and spherical diameter as characteristic length yields

$$N_{St,\infty}\sqrt{R_{D,\infty}} = \frac{h}{\rho_\infty V_\infty c_{p,\infty}}\sqrt{\frac{\rho_\infty V_\infty D}{\mu_\infty}} = 0.763\left(N_{Pr,l}\right)^{-3/5}\left(\frac{c_{p,l}}{c_{p,\infty}}\right)\left(\frac{\rho_l V_l \mu_l}{\rho_\infty V_\infty \mu_\infty}\right)^{1/2}\left(\frac{D}{s}\right)^{1/2} \tag{7}$$

The laminar theory curves shown in figures 5 and 6 were calculated using equations (5) and (7). Local flow conditions were evaluated from isentropic-flow relations and the modified Newtonian pressure distributions.

Turbulent flow.- The theoretical heat-transfer distributions for turbulent flow shown in figures 5 and 6 were obtained from a modification of Falkner's theory given in reference 3 for a sphere. The relation is given as the product of the local Stanton number and $\sqrt{R_s}$ as follows:

$$N_{St,l}\sqrt{R_s} = \frac{h}{\rho_w V_l c_{p,l}}\sqrt{\frac{\rho_w V_l s}{\mu_w}} = 0.0157\left(\frac{\rho_w V_l s}{\mu_w}\right)^{5/14} \tag{8}$$

In this expression, the physical properties of the air are evaluated at the wall with s as characteristic length. Transformation to D as characteristic length and to undisturbed free-stream conditions yields the equation

$$N_{St,\infty}\sqrt{R_{D,\infty}} = 0.0157\left(\frac{c_{p,l}}{c_{p,\infty}}\right)\left(\rho_w V_l\right)^{6/7}\left(\frac{D}{\rho_\infty V_\infty \mu_\infty}\right)^{1/2}\left(\frac{s}{\mu_w}\right)^{-1/7} \tag{9}$$

For the turbulent theory curves shown in figures 5 and 6, the local flow conditions were determined from isentropic-flow relations and the modified Newtonian pressure distribution.

REFERENCES

1. Deveikis, William D., and Walker, Robert W.: Effect of Moisture Content on the Structural Integrity of Glass-Fabric-Reinforced Phenolic-Laminate Radomes Subjected to Aerodynamic Heating. NASA TM X-546, 1961.

2. Crawford, Davis H., and McCauley, William D.: Investigation of the Laminar Aerodynamic Heat-Transfer Characteristics of a Hemisphere-Cylinder in the Langley 11-Inch Hypersonic Tunnel at a Mach Number of 6.8. NACA Rep. 1323, 1957. (Supersedes NACA TN 3706.)

3. Beckwith, Ivan E., and Gallagher, James J.: Heat Transfer and Recovery Temperatures on a Sphere With Laminar, Transitional, and Turbulent Boundary Layers at Mach Numbers of 2.00 and 4.15. NACA TN 4125, 1957.

4. Diaconis, N. S., Wisniewski, Richard J., and Jack, John R.: Heat Transfer and Boundary-Layer Transition on Two Blunt Bodies at Mach Number 3.12. NACA TN 4099, 1957.

5. Jack, John R., Wisniewski, Richard J., and Diaconis, N. S.: Effects of Extreme Surface Cooling on Boundary-Layer Transition. NACA TN 4094, 1957.

6. Cooper, Morton, Mayo, Edward E., and Julius, Jerome D.: The Influence of Low Wall Temperature on Boundary-Layer Transition and Local Heat Transfer on 2-Inch-Diameter Hemispheres at a Mach Number of 4.95 and a Reynolds Number Per Foot of 73.2×10^6. NASA TN D-391, 1960.

7. Braslow, Albert L., Knox, Eugene C., and Horton, Elmer A.: Effect of Distributed Three-Dimensional Roughness and Surface Cooling on Boundary-Layer Transition and Lateral Spread of Turbulence at Supersonic Speeds. NASA TN D-53, 1959.

8. Bidwell, Jerold M.: Use of the Roughness Criterion to Refute Roughness as the Cause of Reported Transition Reversal. Jour. Aero/Space Sci., vol. 27, no. 8, Aug. 1960, pp. 622-623.

9. Stetson, Kenneth F.: Boundary-Layer Transition on Blunt Bodies With Highly Cooled Boundary Layers. Jour. Aero/Space Sci., vol. 27, no. 2, Feb. 1960, pp. 81-91.

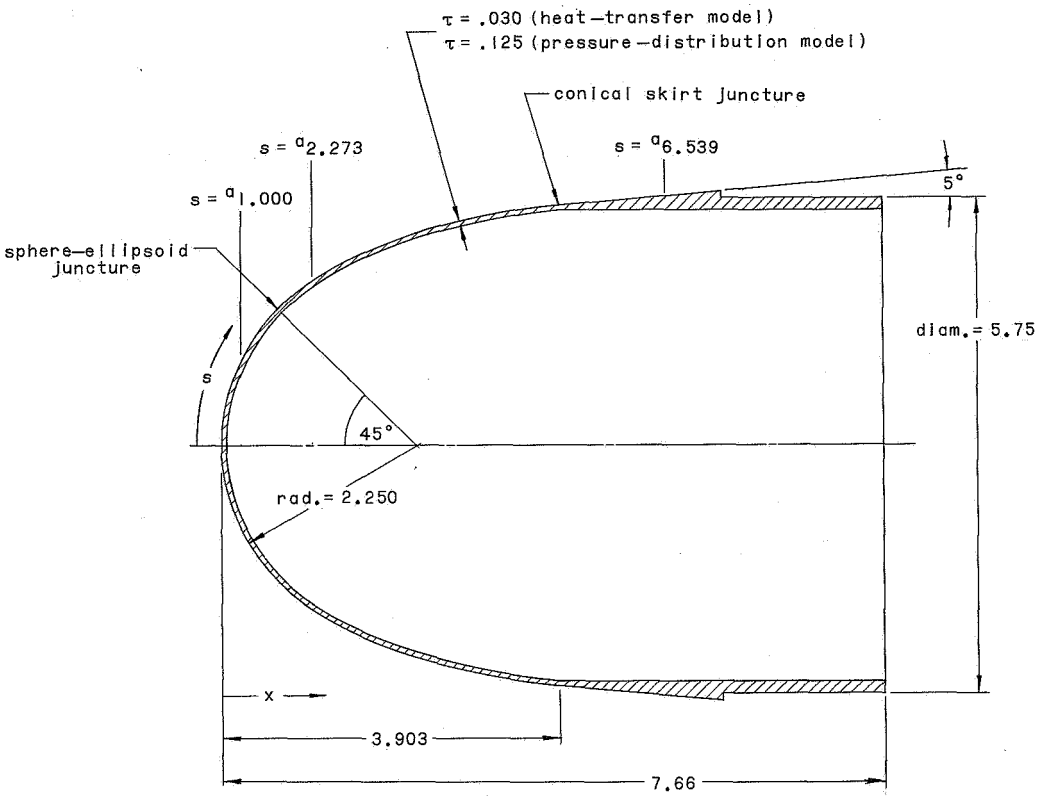

[a]Surface stations on pressure–distribution model with 4 equally spaced orifices.

Thermocouple and orifice locations															
s	[b]0	.250	[b].500	.750	[b]1.000	1.250	1.500	[b]1.750	2.024	[b]2.273	2.509	[b]3.068	[b]3.705	[b]4.537
x	0	.014	.055	.124	.219	.338	.482	.647	.850	1.050	1.250	1.750	2.350	3.150
r	0	.250	.496	.736	.967	1.187	1.391	1.579	1.762	1.911	2.037	2.286	2.501	2.690

[b]Orifice locations on pressure–distribution model.

Figure 1.- Dimensions of model and instrumentation locations. Dimensions are in inches.

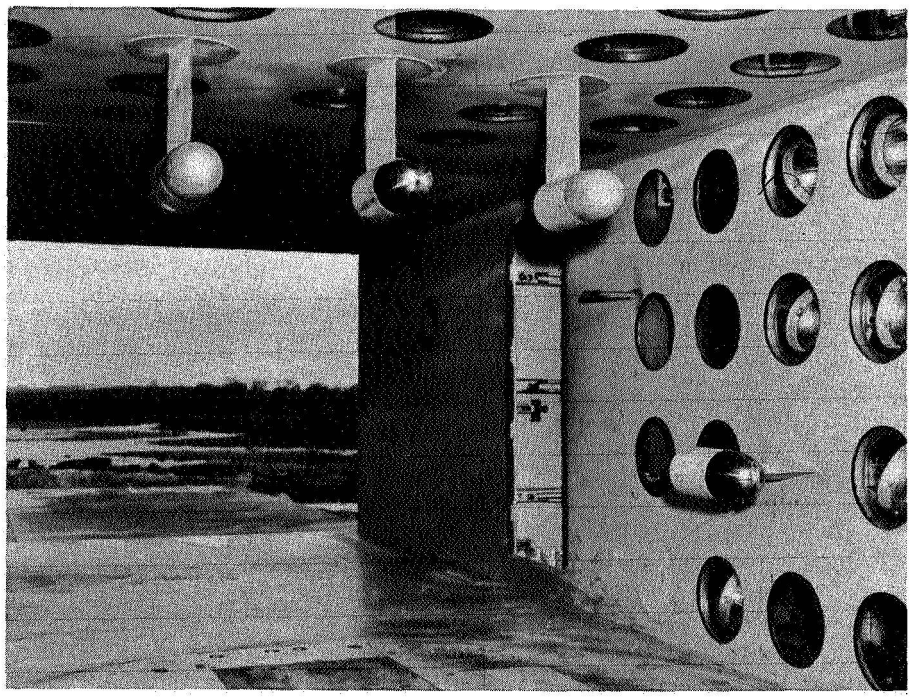

L-60-1502.1

Figure 2.- Model installation in test section viewed from upstream.

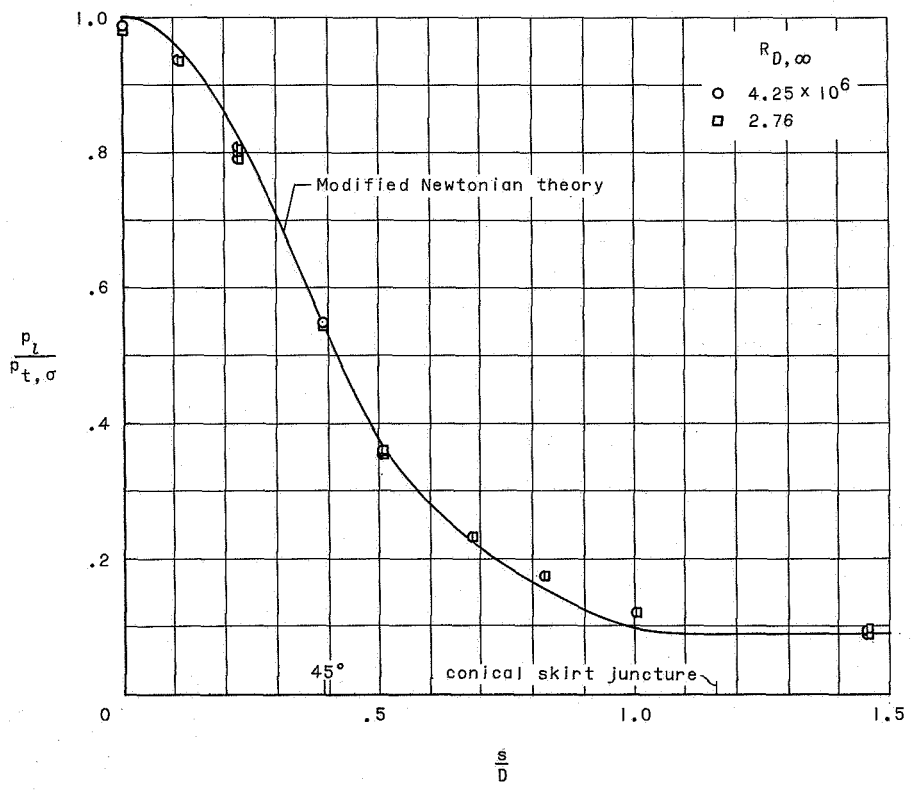

Figure 3.- Variation of the local pressure ratio along the surface.

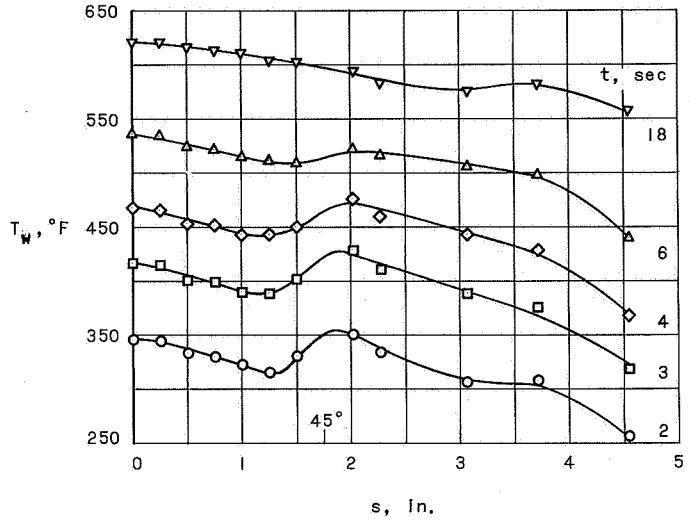

(a) 5 microinches; $R_{D,\infty} = 4.25 \times 10^6$.

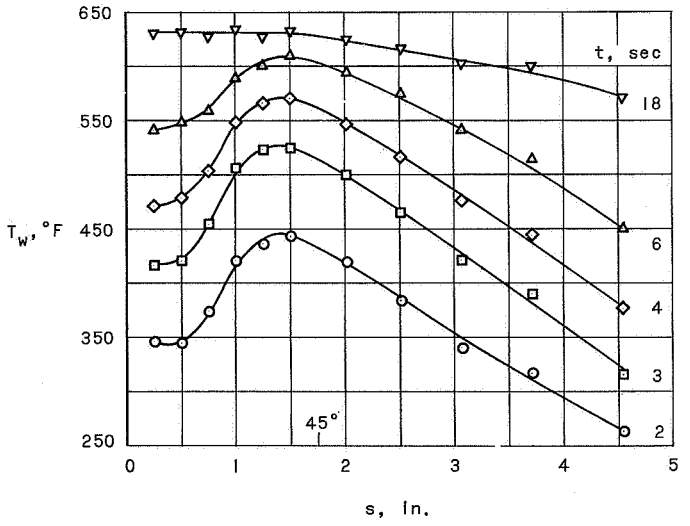

(b) 100 microinches; $R_{D,\infty} = 4.25 \times 10^6$.

Figure 4.- Surface temperature distributions obtained at various times from three sphere-ellipsoid models finished to different surface roughness heights; times shown are based on time zero equal to 0.5-second test time; Mach number 3.0; $T_t = 650^\circ$ F.

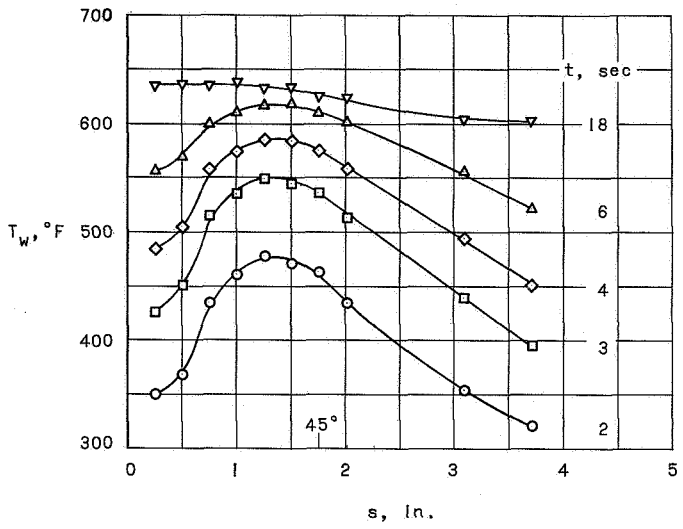

(c) 200 microinches; $R_{D,\infty} = 4.25 \times 10^6$.

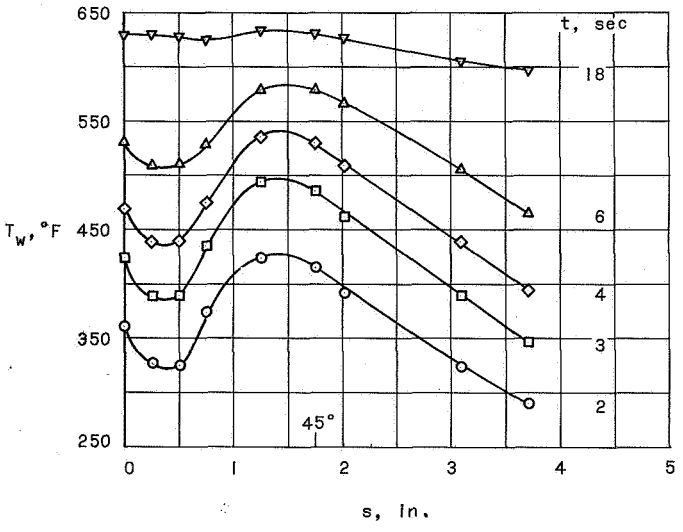

(d) 200 microinches; $R_{D,\infty} = 2.76 \times 10^6$.

Figure 4.- Concluded.

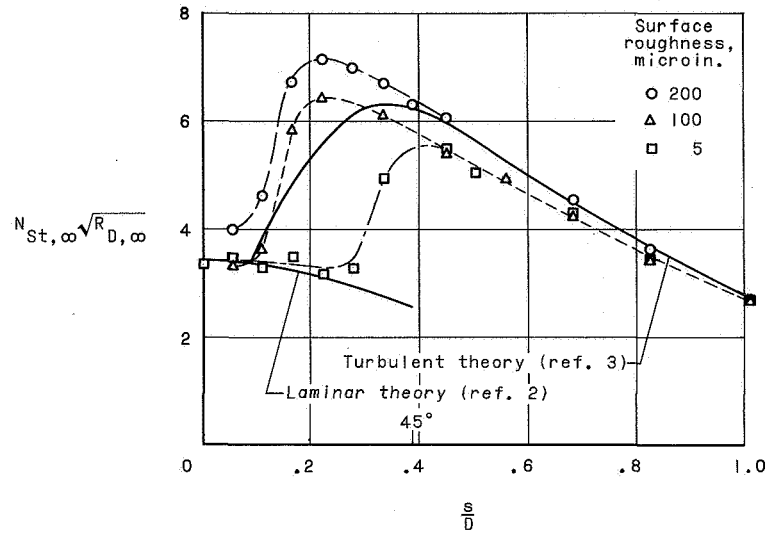

(a) $R_{D,\infty} = 4.25 \times 10^6$; $p_t = 202$ psia; $T_t = 650°$ F.

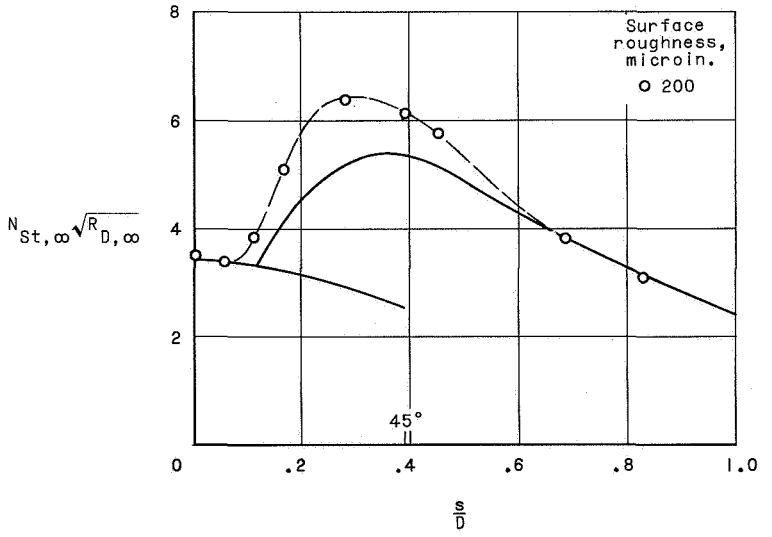

(b) $R_{D,\infty} = 2.76 \times 10^6$; $p_t = 132$ psia; $T_t = 650°$ F.

Figure 5.- The effect of surface roughness on the initial heat-transfer distribution along a sphere-ellipsoid body at Mach number 3.0.

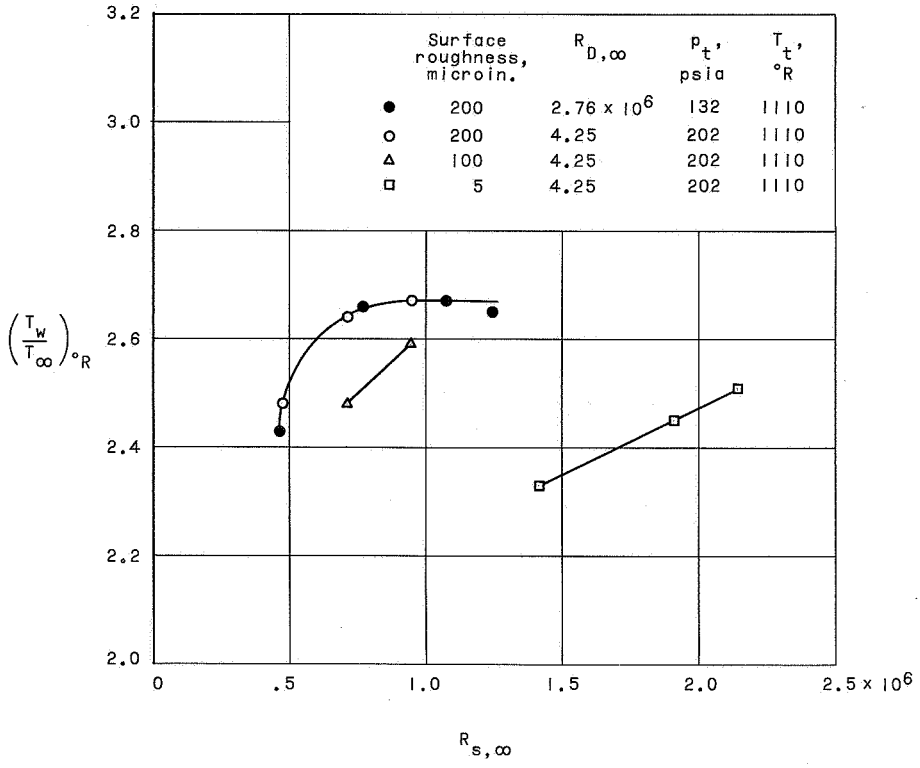

Figure 6.- Variation of model wall temperature for reduction in heating rate with free-stream Reynolds number based on surface distance from the stagnation point on sphere-ellipsoid bodies for different surface roughness conditions; spherical radius, 2.25 inches.

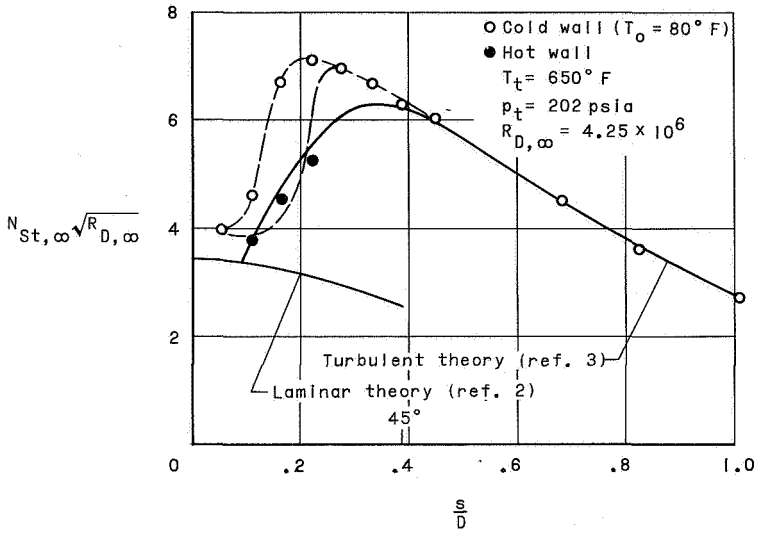

(a) 200 microinches.

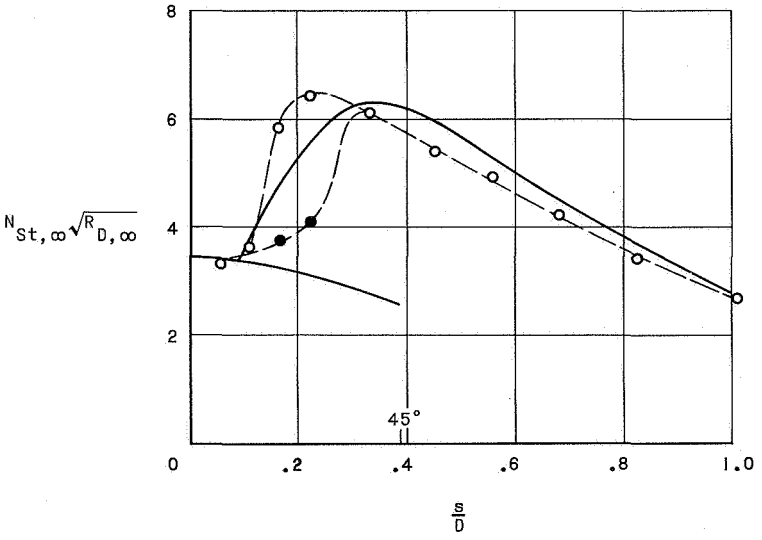

(b) 100 microinches.

Figure 7.- The effect of increasing wall temperature on the local heat transfer to sphere-ellipsoid bodies with different surface roughness conditions.

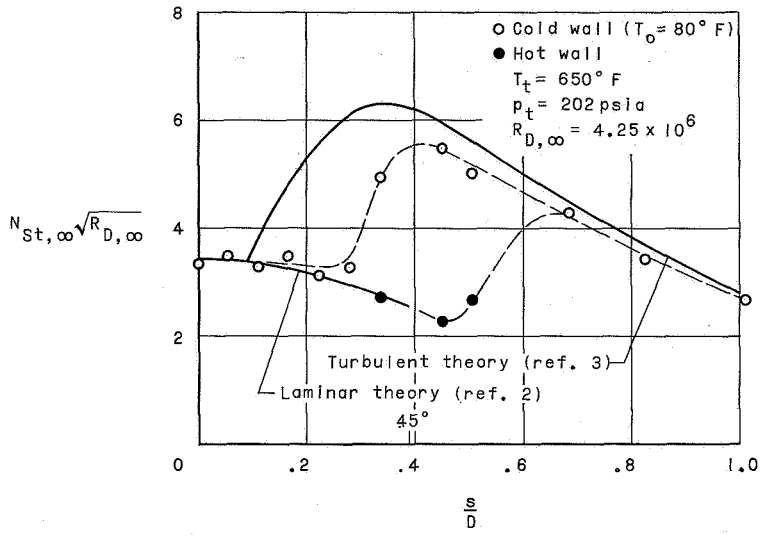

(c) 5 microinches.

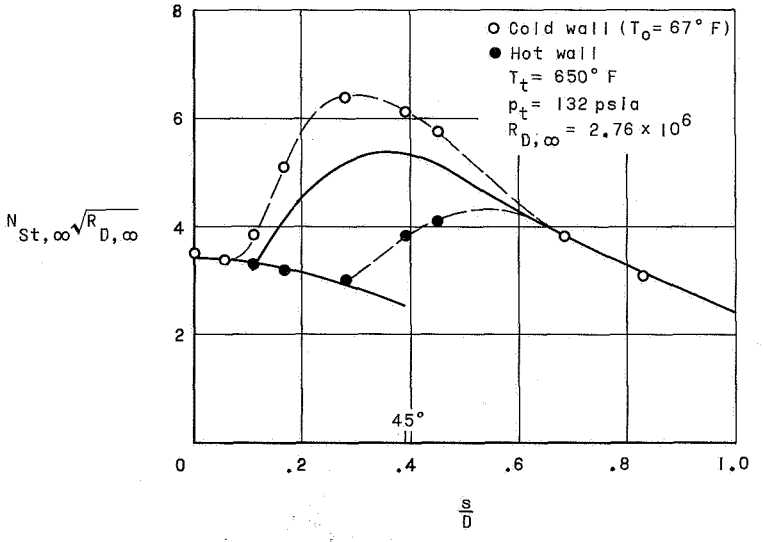

(d) 200 microinches.

Figure 7.- Concluded.

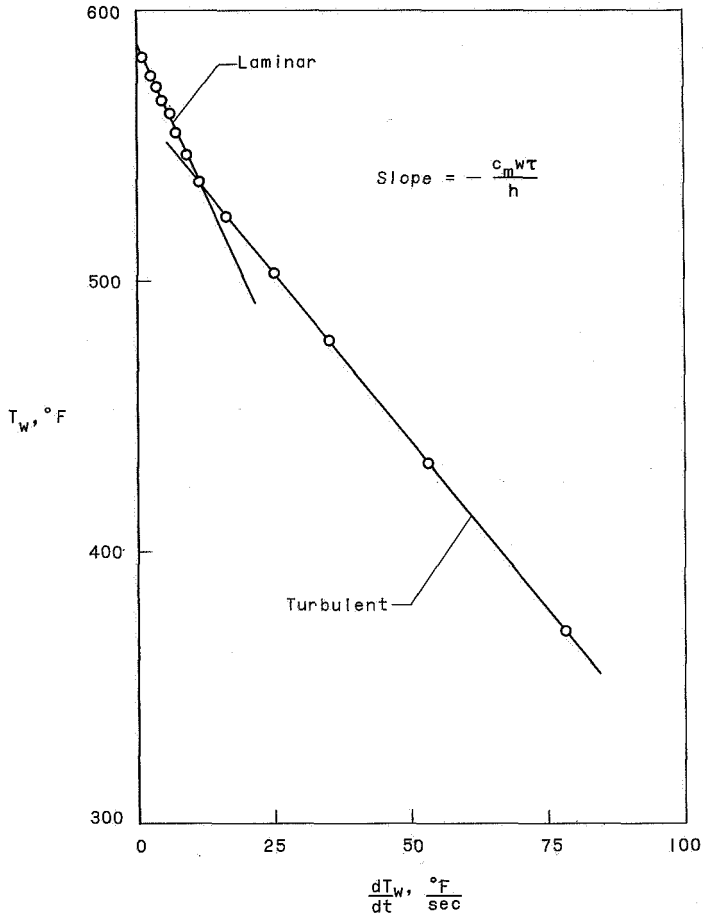

Figure 8.- Method for determining experimental heat-transfer coefficients from thermocouple data; illustration of transition from turbulent to laminar flow of the smooth model at s = 2.273 inches.